Int Nano Lett (2015) 5:85–92
DOI 10.1007/s40089-015-0141-z

ORIGINAL ARTICLE

# Synthesis of $Fe_3O_4$ nanoparticles and its antibacterial application

**Y. T. Prabhu · K. Venkateswara Rao · B. Siva Kumari · Vemula Sesha Sai Kumar · Tambur Pavani**

Received: 30 November 2014 / Accepted: 12 February 201521 February 2015Published online: 21 February 2015


**Abstract** The Present work outlines the antibacterial activity of $Fe_3O_4$ nanoparticles synthesized through chemical combustion method where ferric nitrate is used as precursor material and urea as fuel with the assistant of Tween 80, a non-ionic surfactant. The obtained $Fe_3O_4$ nanoparticles were characterized by X-ray diffraction, differential thermal analysis/thermo gravimetric analysis (DTA/TGA), particle size analyzer, SEM with EDAX and TEM. Various parameters such as dislocation density, micro strain, analysis of weight loss and surface morphological studies were calculated. The particle size was calculated from XRD and it was found to be 33–40 nm. Using well diffusion method antibacterial activity of $Fe_3O_4$ nanoparticles was tested against gram-positive and gram-negative *Staphylococus aureus*, Xanthomonas, *Escherichia coli* and *Proteus vulgaris*. $Fe_3O_4$ nanoparticles exhibited strong antibacterial activity against bacterial species.

**Keywords** $Fe_3O_4$ nanoparticles · XRD · TG/DTA · TEM · SEM · EDAX · Antibacterial activity

## Introduction

Nano materials are widely synthesized for their properties like optical, mechanical and magnetic properties to counter the bulk materials [1–3]. Metal oxides are used in various applications like magnetic storage, catalysis and biological applications like bone tissue engineering [4–7]. The prolonged life expectation and aging of population has brought the escalating request of artificial material to regenerate diseased bones [8–11]. Nanotechnology has responded to the situation with various ceramics with its bioactivity [12], mechanical properties [13, 14] and ability to kindle bone growth. In particular iron oxide powder at nanometer is utilized at length because of the development in preparation technology. Monodispersed magnetite nanoparticles have given a new impetus in the application field where magnetic nanoparticles are extensively used in Ferro fluids, biological imaging and therapies [15, 16]. Magnetic iron oxide ($Fe_3O_4$) with oxygen forming face centred cubic has a cubic inverse spinal structure and in the interstitial tetrahedral sites and octahedral sites are occupied by iron (Fe) cations [17]. At the room temperature $Fe^{+2}$ and $Fe^{+3}$ ions flip between themselves in the octahedral sites giving rise to a class called half-metallic materials [18]. The desired physical and chemical properties of magnetite nanoparticles are synthesized by several chemical synthetic routes like co-precipitation of aqueous ferrous and ferric solutions [19], microemulsion technique [20] and hydrothermal synthesis [21]. Superparamagnetic nanoparticles are highly exciting materials because of their uses in magnetic resonance imaging (MRI) [22–26], drug delivery [27] and cell separation [28]. In the area of antibacterial agents metal nanoparticles are of a particular interest because they could be synthesized with high surface area with highly potential active sites [29]. A distinct class of metal oxide with distinctive magnetic properties and superior biocompatibility are is found in iron oxide nanoparticles.

In the past few years, a wide range of work has been done in producing new drugs due to the resistance of

Y. T. Prabhu (✉) · K. V. Rao · V. S. S. Kumar · T. Pavani
Centre for Nano Science and Technology, Institute of Science and Technology, Jawaharlal Nehru Technological University Hyderabad, Hyderabad, India
e-mail: ytprabhusj@gmail.com

B. S. Kumari
Department of Botany, Andhra Loyola College, Vijayawada, Andhra Pradesh, India

micro-organisms to the current drugs. This work is a novel way of synthesizing $Fe_3O_4$ nanoparticles with the surfactant; and it is also an attempt to study the antibacterial properties of $Fe_3O_4$ nanoparticles.

## Materials and methods

### Materials

The chemical reagents used in this work were ferric nitrate, surfactant Tween 80, Urea and ammonia solution. Analytical grade chemical reagents were used throughout the experiment. We have taken four bacterial species, gram-positive *Staphylococus aureus* and gram-negative Xanthomonas, *Escherichia coli* and *Proteus vulgaris*. The microbes were acquired from the biotechnology department of Jawaharlal Nehru Technological University Hyderabad.

### Synthesis

The synthesis of magnetite ($Fe_3O_4$) Nanoparticles was done by chemical combustion. The required amount of ferric nitrate (0.1 M) was dissolved in 20 ml of deionized water under the magnetic stirrer for 10 min. The fuel urea and ammonia (0.1 M) were dissolved separately in 30 ml of distilled water, respectively. The surfactant TWEEN80 (0.07 M) was dissolved in 20 ml of distilled water and was kept under stirring for 10 min separately. Fuel solution was mixed with oxidizer solution which was under stirring followed by mixing of surfactant solution. The whole solution was kept under stirring for 15 min for stirring. The solution was placed on a hot plate to initiate the reaction. When the temperature had started to increase, the solution boiled and fumes gushed forth from the solution; as the temperature increased above 100 °C, the solution started to evaporated leading to an increase in the viscosity of the liquid and smouldering started eventually self-ignition took place forming the final product ($Fe3O_4$). The powder was collected from the beaker and calcinated for 1 h at 400 °C. The powder It was collected for characterization and antibacterial application.

### Screening of antibacterial activities

The well-diffusion technique [30] was used. 500 µl of microbes cultures of age 18–24 h were added to Petri plates and nutrient agar was poured. Once the medium was solidified, holes were made and each hole was packed with different concentrations of nanoparticles ranging from 20 to 150 µg/ml one after the other. The plates were wrapped in parafilm tape and transferred to incubator and maintained at 37 °C for 24 h. Negative and positive controls were used. The inhibition zones of were then recorded in centimetres.

## Results and discussion

### XRD

An X-ray diffraction (XRD) pattern of the sample was done at room temperature on D8 Advance Bruker diffractometer with a Cu Kα radiation ($\lambda = 0.154$ nm). From Fig. 1, it can be observed that the diffraction peaks exhibit a phase face centred cubic structure and was in good agreement with the JCPDS [space group Fd3m (227), JCPDS #89-4319]. Using Scherrer formula [31, 32], average crystallite sizes were estimated. It was found that the size of nanoparticles were 33–40 nm from the X-ray line broadening.

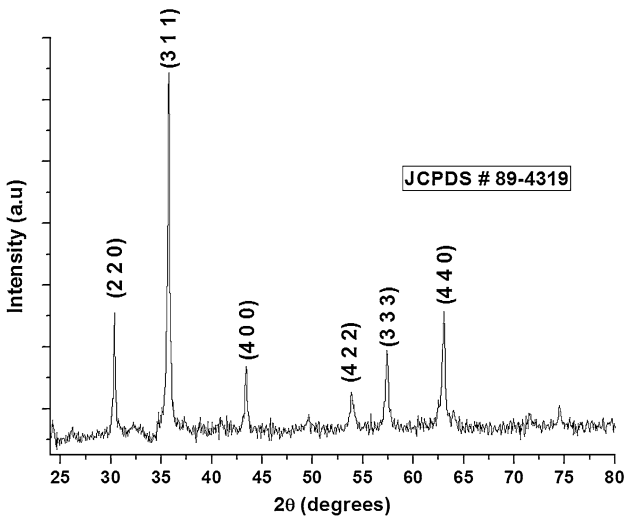


**Fig. 1** XRD patterns of $Fe_3O_4$

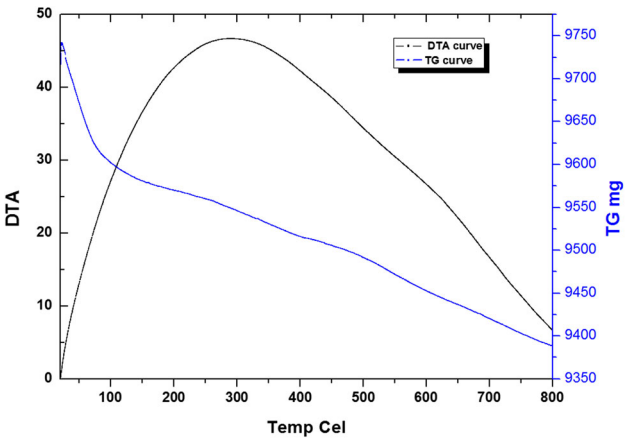


**Fig. 2** TG/DTA of $Fe_3O_4$

**Table 1** The values of standard '*d*', observed '*d*', absolute '*a*' difference, percentage of lattice contraction, crystalline size, dislocation density, strain and *h*, *k*, *l* of $Fe_3O_4$

| Observed $2\theta$ (°) | Standard d (Å) $a = 8$ 3952 (Å) | Observed d (Å) $a = 8$ 3308 (aureus bacterial strains.Å) | Absolute '*a*' diffrence | % of lattice contraction | Crystalline size | Dislocation density ($\delta$) ($\times 10^{15}$) lines/m$^2$ | Strain ($\varepsilon$) ($\times 10^{-3}$) lines/m$^4$ | *h* | *k* | *l* |
|---|---|---|---|---|---|---|---|---|---|---|
| 30.34 | 2.968 | 2.94541 | 0.02259 | 2.259 | 42.71 | 5.48 | 8.11 | 2 | 2 | 0 |
| 35.72 | 2.531 | 2.51185 | 0.01915 | 1.915 | 36.54 | 7.48 | 9.48 | 3 | 1 | 1 |
| 43.4 | 2.098 | 2.08272 | 0.01528 | 1.528 | 37.89 | 6.96 | 9.91 | 4 | 0 | 0 |
| 53.92 | 1.713 | 1.70053 | 0.01247 | 1247 | 17.68 | 21.9 | 19.58 | 4 | 2 | 2 |
| 57.39 | 1.615 | 1.60328 | 0.01172 | 1.172 | 34.6 | 834 | 10.01 | 3 | 3 | 3 |
| 63.01 | 1.484 | 1.47271 | 0.01129 | 1.129 | 33.54 | 8.88 | 103 | 4 | 4 | 0 |

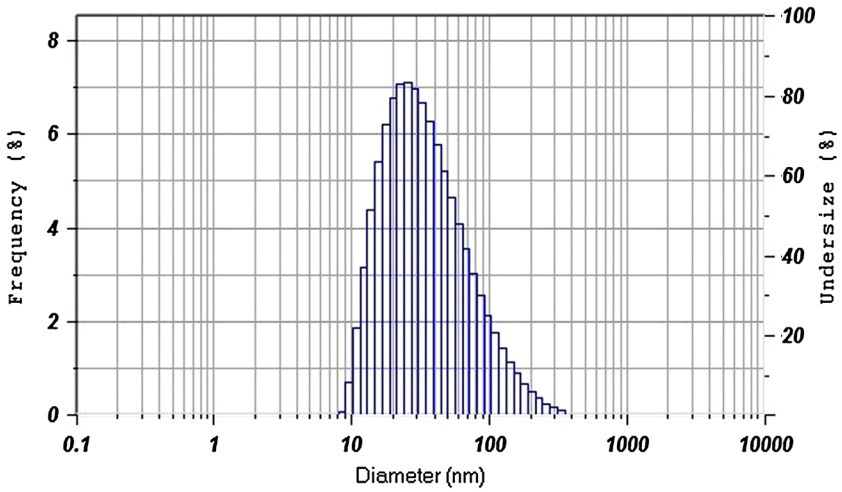


**Fig. 3** Particle analyzer of $Fe_3O_4$

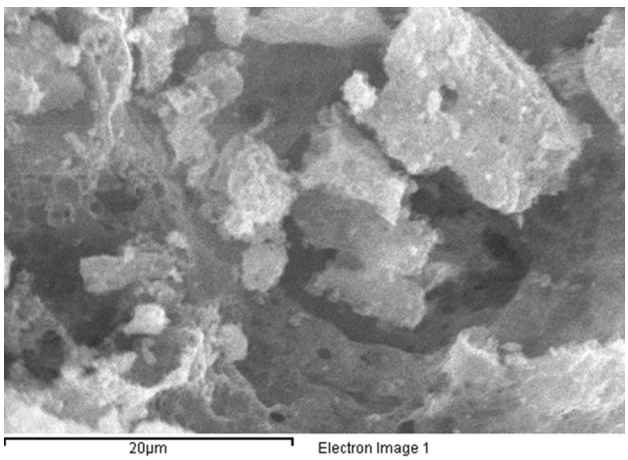


**Fig. 4** SEM image of $Fe_3O_4$

$$D = \frac{0.9\lambda}{\beta \cos\theta} \quad (1)$$

Where $\lambda$ is the X-ray wavelength (1.54 Å) for copper Kα. $\theta$ is the Bragg's angle. $\beta$ is full width half maximum

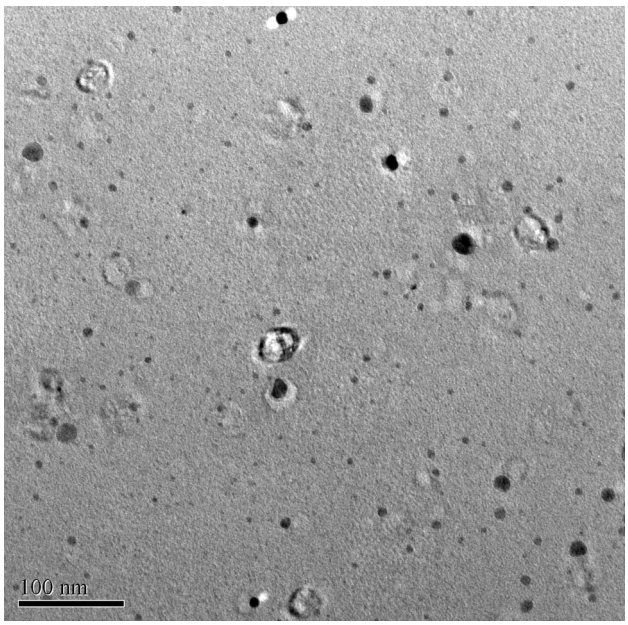


**Fig. 5** TEM image of $Fe_3O_4$

value. Dislocation density ($\delta$) is calculated with the crystalline size.

$$\delta = \frac{1}{D^2} \tag{2}$$

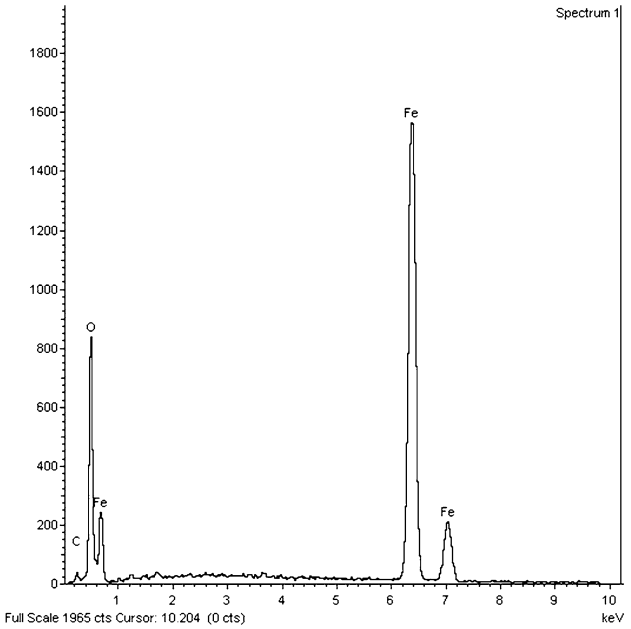


**Fig. 6** EDAX of $Fe_3O_4$

From the calculated $d$ spacing value, the lattice constants are calculated as follows: with the below formulae.

$$d^2 = \frac{a^2}{h^2} + \frac{b^2}{k^2} + \frac{c^2}{l^2} \tag{3}$$

where $a$, $b$, $c$ are lattice parameters and $h$, $k$, $l$ are miller indices.

Micro strain arises due to the lattice misfit which varies on the deposition conditions and thus it is calculated by the formula.

$$\varepsilon = \frac{(\beta \cos \theta)}{4} \tag{4}$$

We have observed that dislocation density has decreased with the increase in the crystallite size. Similarly, the micro strain has increased with the decrease in the crystallite size. These results are shown in the Table 1.

## TG/DTA

In the differential thermal analysis/thermogravimetric analysis (DTA/TG), we have observed both exothermic and endothermic graphs. There is a gradual weight loss in the TG graph as the temperature increases. At 100 °C, there was a sudden fall in the graph indicating that there

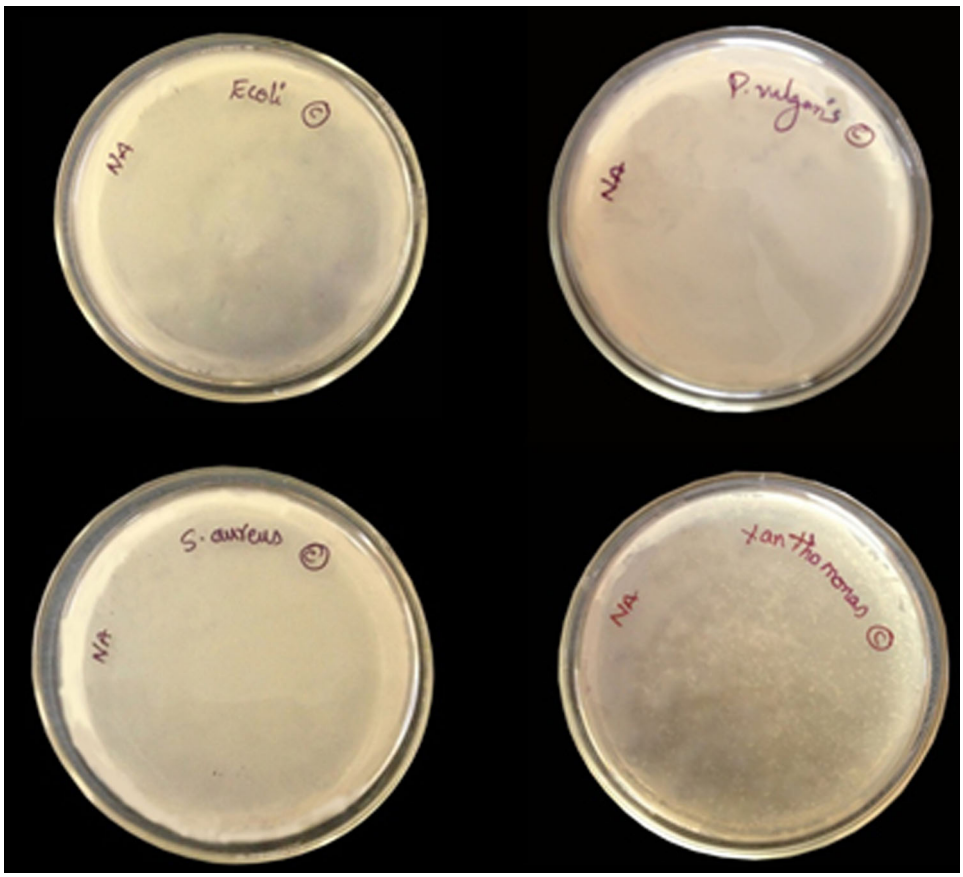


**Fig. 7** Antimicrobial activity of $Fe_3O_4$ at control level

was weight loss due to the loss of moisture in the sample. There was gradual weight loss due to the loss of carbon at 500 °C. Correspondingly, in Fig. 2, there was DTA graph showing the endothermic peak at 350 °C indicating that maximum heat was absorbed into the sample.

## Particle size analyzer

The particle size was calculated at various cumulative factors using particle analyser. In ethyl alcohol at room temperature and at low concentration the sample was suspended and ultra sonicated for 10 min and subjected to laser of 245 nm wavelength in the particle analyser instrument. Thus in Fig. 3 average particle size for sample was shown with histogram.

## SEM, TEM and EDAX

The morphological studies were done by using SEM. In Fig. 4, we have observed that the sample has many pores on the surface of the sample indicating that the obtained sample has porous nature.

The main benefit of a TEM is that it can simultaneously give evidence in real space (in the imaging mode) and reciprocal space (in the diffraction mode). Using the TEM image, both the size and shape of the obtained nanoparticles were observed. They were spherical in shape and porous surface as seen in the Fig. 5. The crystallite size obtained by the Scherrer's formula and the size from the TEM confirm each other.

The energy-dispersive X-ray spectroscopy results are shown in the Fig. 6. It shows the presence of oxygen and iron. This confirms the existence of oxygen and iron in the sample (Fig. 6).

## Antibacterial activity

$Fe_3O_4$ showed antibacterial effect against gram-positive as well as gram-negative bacteria which clearly indicates that these nanoparticles are effective antibacterial agents. In Figs. 7, 8 and 9 the control, low and high concentrations of $Fe_3O_4$ were shown, respectively. Many antibacterial studies were made using different nanoparticles. The reason for the bactericidal activity is due to the presence of reactive oxygen species (ROS) generated by different nanoparticles [33]. Chemical interaction between hydrogen peroxide and membrane proteins or between the chemical produced in the presence of $Fe_3O_4$ nanoparticles and the outer bilayer

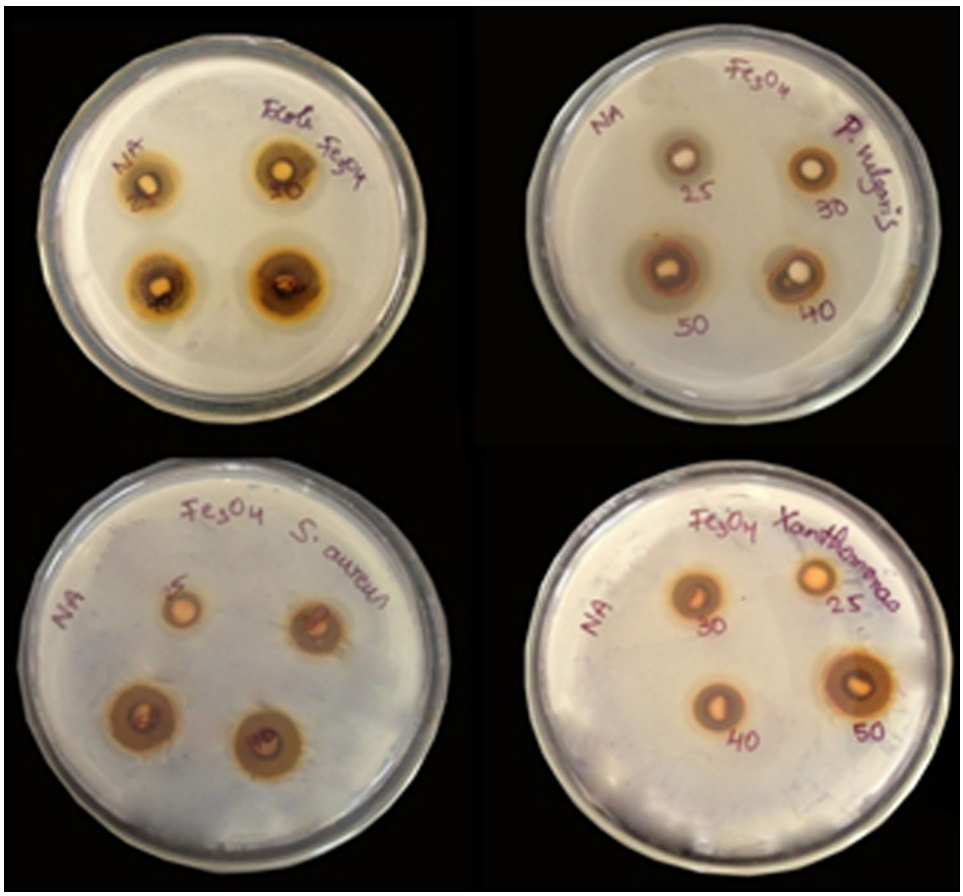


**Fig. 8** Antimicrobial activity of different extracts with $Fe_3O_4$ at low concentration

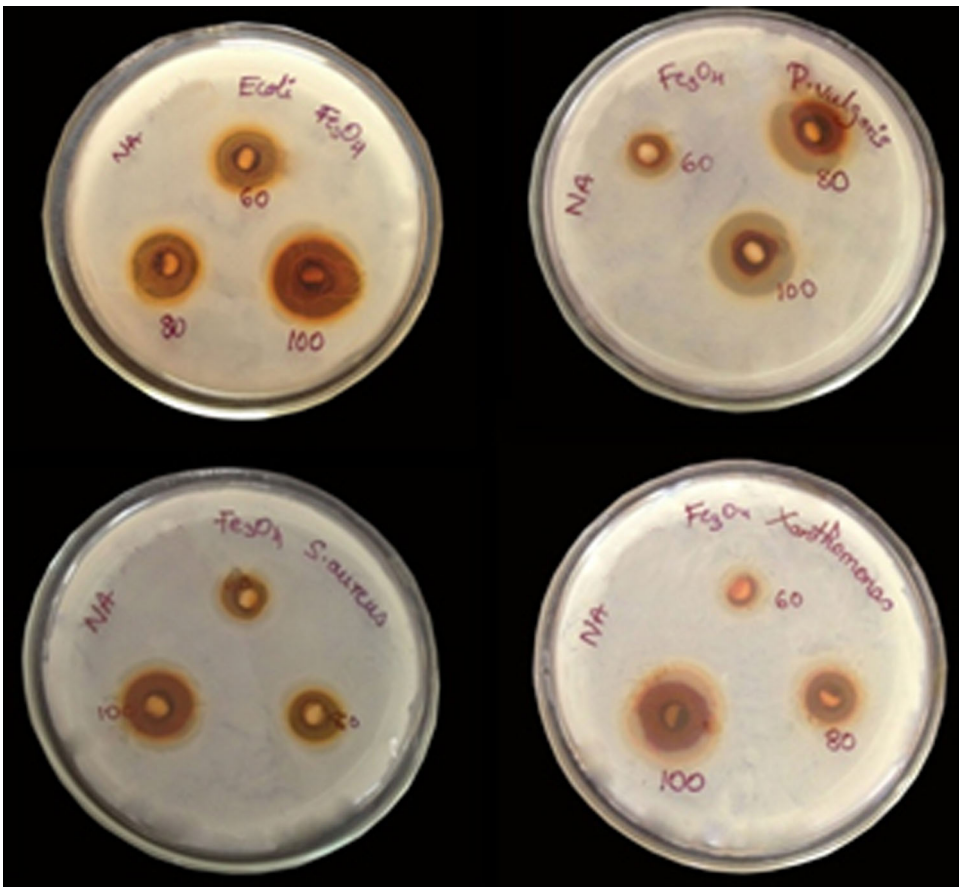


**Fig. 9** Antimicrobial activity of different extracts with $Fe_3O_4$ at high concentration

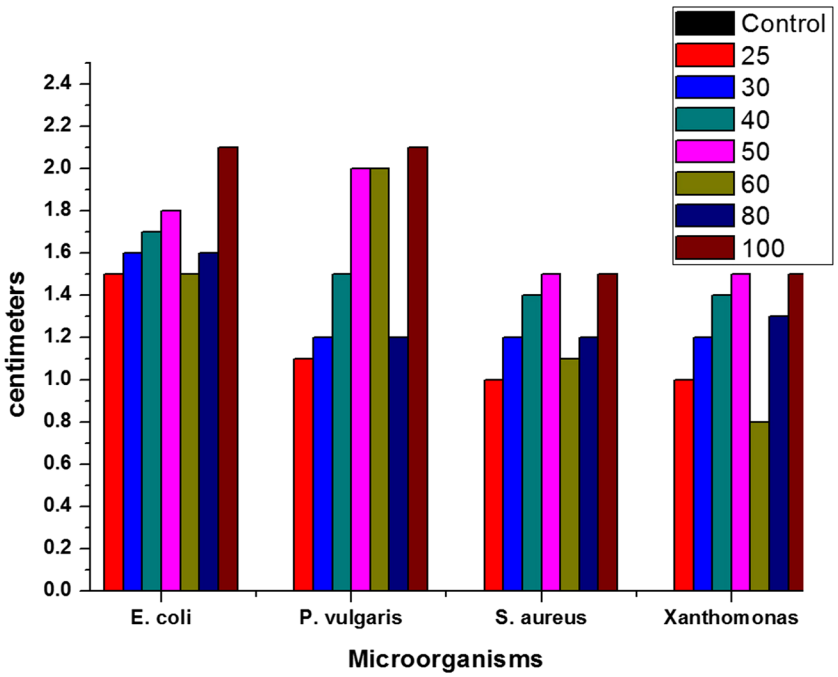


**Fig. 10** Activation index against various microorganisms

of bacteria could be the reason for the antibacterial activity of $Fe_3O_4$. The hydrogen peroxide produced enters the cell membrane of bacteria and kills them. It is also noted that nanoparticles continue to be in interaction with dead bacteria once the hydrogen peroxide is generated; thus foiling further bacterial action and continue to produce and release

hydrogen peroxide to the medium [34]. In Figs. 8 and 9 we clearly see the antibacterial activity in brown and yellow colours indicating that the bacteria is completely destroyed and antibacterial activity is still active, respectively.

The possible mechanism of action is that the metal nanoparticles are carrying the positive charges and the microbes are having the negative charges which create the electromagnetic attraction between the nanoparticles and the microbes. When the attraction is made, the microbes get oxidized and die instantly [35]. Generally, the nanomaterials release ions, which react with the thiol groups (–SH) of the proteins present on the bacterial cell surface which leads to cell lysis [36].

The central mechanism that caused the antibacterial activity by the particles might be through oxidative stress caused by ROS [37, 38]. ROS includes radicals like superoxide radicals ($O_2^-$), hydroxyl radicals (–OH) and hydrogen peroxide ($H_2O_2$); and singlet oxygen ($^1O_2$) could be the reason damaging the proteins and DNA in the bacteria. ROS could have been produced by the present metal oxide (iron oxide) leading to the inhibition of most pathogenic bacteria like *S. aureus*, Xanthomonas, *E. coli* and *P. vulgaris*. A related study was explained by Kim et al. [16] in which hydrogen peroxide ($H_2O_2$) was generated when $Fe^{2+}$ responded with oxygen. The ferrous irons reacted with the produced $H_2O_2$ subsequently through Fenton reaction and thus leading to creating hydroxyl radicals which damage the biological macro-molecules [39].

The nanoparticles can also produce bactericidal effects as verified by a few authors have verified. A few authors like Lee et al. [40] stated that the iron nanoparticles caused the inactivation of *E. coli* by zero-valent and the diffusion of the small particles ranging from 10 to 80 nm into *E. coli* membranes. Nano scale zero valent iron could interact with intracellular oxygen thus generating oxidative stress and ultimately triggering the interference of the cell membrane. Nanoparticles of ZnO and MgO also have revealed that with a decrease in particle size, antibacterial activity increases [41, 42]. Likewise, Taylor and Webster also made a study studies on iron oxide nanoparticles and its bactericidal effects of on *S. epidermidis* [43]. They also described that bacterial inhibition depends on concentration. We need to note that iron oxide nanoparticles do not negatively impact all cells but with an appropriate magnetic field of iron oxide, nanoparticles may be engaged to destroy bacteria.

The results revealed that the microorganisms are sensitive to the test samples in varying magnitudes. The Antibacterial activity of $Fe_3O_4$ nanoparticles on 4 bacterial strains is summarized in Fig. 10. The $Fe_3O_4$ Nanoparticle showed a good antibacterial activity on *E. coli* and *P. vulgaris* than the *S. aureus* bacterial strains. The gram-negative bacteria are more sensitive when compared to gram-positive bacteria. Earlier studies also indicate that gram-negative bacteria are less sensitive than gram-positive bacteria. A strong bactericidal activity was observed against *E. coli* and *P. vulgaris*.

## Conclusion

The novel facile Surfactant TWEEN80 has been used to synthesis $Fe_3O_4$ for the first time with fuel urea. The XRD result and TEM results confirmed $Fe_3O_4$ has the crystallite size 35 nm. The differential thermal analysis/thermogravimetric analysis showed the weight due to vapour and carbon. The dislocation density has decreased with the increase in the crystallite size. Similarly the micro strain has increased with the decrease in the crystallite size. The $Fe_3O_4$ nanoparticles showed their antibacterial properties on both gram positive and gram negative bacterial strains. As the diameter of the zone of inhibition is high, we can conclude that $Fe_3O_4$ is a very effective antibacterial agent.



## References

1. Siegel RW. In: Siegel RW, Hu E, Roco MC (eds) Nanostructure science and technology. A worldwide study. WTEC, Loyola College in Maryland (1999)
2. Zhou, K., Wang, R., Xu, B., Li, Y.: Synthesis, characterization and catalytic properties of CuO nanocrystals with various shapes. Nanotechnology **17**, 3939 (2006)
3. Xin-ling, G.E.N.G., Zheng-tao, S.U.: Research on preparation of nano-copper powder by liquid-phase method. Appl Chem Ind **34**(10), 615–617 (2005)
4. Sadeghpour, S., Amirjani, A., Hafezi, M., Zamanian, A.: Fabrication of a novel nanostructured calcium zirconium silicate scaffolds prepared by a freeze-casting method for bone tissue engineering. Ceram Int **40**, 16107–16114 (2014)
5. Furno, F., Morley, K.S., Wong, B., Sharp, B.L., Arnold, P.L., Howdle, S.M., Bayston, R., Brown, P.D., Winship, P.D., Reid, H.: Silver nanoparticles and polymeric medical devices: a new approach to prevention of infection? J Antimicrob Chem **54**, 1019 (2004)
6. Jeong, S.H., Yeo, S.Y., Yi, S.C.: The effect of filler particle size on the antibacterial properties of compounded polymer/silver fibers. J Mater Sci **40**, 5407 (2005)
7. Hsiao, M.T., Chen, S.F., Shieh, D.B., Yeh, C.S.: One-pot synthesis of hollow $Au_3Cu_1$ spherical-like and biomineral botallackite $Cu_2(OH)_3Cl$ flowerlike architectures exhibiting antimicrobial activity. J Phys Chem B **110**, 205 (2006)
8. Hutmacher, D.W.: Scaffolds in tissue engineering bone and cartilage. Biomaterials **21**, 2529–2543 (2000)
9. Mirhadi, S., Tavangarian, F., Emadi, R.: Synthesis, characterization and formation mechanism of single-phase nanostructure bredigite powder. Mater Sci Eng C **32**, 133–139 (2012)

10. Tavangarian, F., Li, Y.: Carbon nanostructures as nerve scaffolds for repairing large gaps in severed nerves. Ceram Int **38**, 6075–6090 (2012)
11. Zreiqat, H., Ramaswamy, Y., Wu, C., Paschalidis, A., Lu, Z., James, B., Birke, O., McDonald, M., Little, D., Dunstan, C.R.: The incorporation of strontium and zinc into a calcium–silicon ceramic for bone tissue engineering. Biomaterials **31**, 3175–3184 (2010)
12. Tavangarian, F., Emadi, R.: Nanostructure effects on the bioactivity of forsterite bioceramic. Mater Lett **65**, 740–743 (2011)
13. Emadi, R., Tavangarian, F., Esfahani, S.I.R., Sheikhhosseini, A., Kharaziha, M.: Nanostructured forsterite coating strengthens porous hydroxyapatite for bone tissue engineering. J Am Ceram Soc **93**, 2679–2683 (2010)
14. Roohani-Esfahani, S., Dunstan, C.R., Davies, B., Pearce, S., Williams, R.: Repairing a critical-sized bone defect with highly porous modified and unmodified baghdadite scaffolds. Acta Bio Mater **8**, 4162–4172 (2012)
15. Oswald, P., Clement, O., Chambon, C., Schouman-Claeys, E., Frija, C.: Liver positive enhancement after injection of superparamagnetic nanoparticles: respective role of circulating and uptaken particles. Magn Reson Imaging **15**, 1025 (1997)
16. Kim, D.K., Zhang, Y., Kehr, J., Klason, T., Bjelke, B., Muhammed, M.: Characterization and MRI study of surfactant-coated superparamagnetic nanoparticles administered into the rat brain. J Magn Magn Mater **225**, 256 (2001)
17. Cornell, R.M., Schwertmann, U.: The iron oxides: structure, properties, reactions, occurrence and uses. VCH, New York (1996)
18. Verwey, E.J.W.: Electronic conduction of magnetite ($Fe_3O_4$) and its transition point at low temperatures. Nature **144**, 327 (1939)
19. Kang, Y.S., Risbud, S., Rabolt, J.F., Stroeve, P.: Synthesis and characterization of nanometer-size $Fe_3O_4$ and $\gamma$-$Fe_2O_3$ particles. Chem Mater **8**, 2209 (1996)
20. Zhou, Z.H., Wang, J., Liu, X., Chan, H.S.O.: Synthesis of $Fe_3O_4$ nanoparticles from emulsions. J Mater Chem **11**, 1704 (2001)
21. Zhou, Z.H., Wang, J., Liu, X., Chan, H.S.O.: Study of higher selectivity to styrene oxide in the epoxidation of styrene with hydrogen peroxide over La-doped MCM-48 catalyst. J Phys Chem C **113**, 7181–7185 (2009)
22. Corot, C., Robert, P., Idée, J.M., Port, M.: Recent advances in iron oxide nanocrystal technology for medical imaging. Adv Drug Deliv Rev **58**, 1471–1504 (2006)
23. Zhao, D.L., Zeng, X.W., Xia, Q.S., Tang, J.T.: Preparation and coercivity and saturation magnetization dependence of inductive heating property of $Fe_3O_4$ nanoparticles in an alternating current magnetic field for localized hyperthermia. J Alloy Comp **496**, 215–218 (2009)
24. Lu, J., Ma, S., Sun, J., Xia, C., Liu, C., Wang, Z., Zhao, X., Gao, F., Gong, Q., Shuai, X., Ai, H., Gu, Z.: Manganese ferrite nanoparticle micellar nanocomposites as MRI contrast agent for liver imaging. Biomaterials **30**, 2919–2928 (2009)
25. Bahadur, D., Giri, J.: Biomaterials and magnetism. Sadhana **28**, 639–656 (2003)
26. Alexiou, C., Arnold, W., Klein, R.J., Parak, F.G., Hulin, P., Bergemann, C., Erhardt, W., Wagenpfeil, S., Lubbe, A.S.: Locoregional cancer treatment with magnetic drug targeting. Cancer Res **60**, 6641–6648 (2000)
27. Sutton, A., Harrison, G.E., Carr, T.E., Barltrop, D.: Reduction in the absorption of dietary strontium in children by an alginate derivative. Br J Radiol **44**, 523 (1971)
28. Cheng, F.Y., Su, C.H., Yang, Y.S., Yeh, C.S., Tsaib, C.Y., Wu, C.L., Wu, M.T., Shie, D.B.: Characterization of aqueous dispersions of $Fe_3O_4$ nanoparticles and their biomedical applications. Biomaterials **26**, 729–738 (2005)
29. Stoimenov, P.K., Klinger, R.L., Marchin, G.L., Klabunde, K.J.: Metal oxide nanoparticles as bactericidal agents. Langmuir **18**(17), 6679–6686 (2002)
30. Chung, K.T., Chen, S.C., Wong, T.Y., Wei, C.I.: Effects of benzidine and benzidine analogues on growth of bacteria including *Azotobacter vinelandii*. Environ Toxicol Chem **17**, 271–275 (1998)
31. Cullity, B.D.: Elements of x-ray diffraction. Addison-Wesley, Philippines (1978)
32. Pal, J., Chauhan, P.: Structural and optical characterization of tin dioxide nanoparticles prepared by a surfactant mediated method. Mater Charact **60**, 1512 (2009)
33. Yamamoto, O.: Influence of particle size on the antibacterial activity of zinc oxide. Int J Inorg Mater **3**(7), 643–646 (2001)
34. Padmavathy, N., Vijayaraghavan, R.: Enhanced bioactivity of ZnO nanoparticles—an antimicrobial study. Sci Technol Adv Mat **9**(3), 35004–35010 (2008)
35. Rezaei-Zarchi, S., Javed, A., Ghani, M.J., Soufian, S., Firouzabadi, F.B., Moghaddam, A.B., Mirjalili, S.H.: Comparative study of antimicrobial activities of $TiO_2$ and CdO nanoparticles against the pathogenic strain of *Escherichia coli*. Iran J Pathol **5**(2), 83–89 (2010)
36. Zhang, H., Chen, G.: Potent antibacterial activities of Ag/$TiO_2$ nanocomposite powders synthesized by a one-pot sol–gel method. Environ Sci Technol **43**(8), 2905–2910 (2009)
37. Mahdy, S.A., Raheed, Q.J., Kalaichelvan, P.T.: Antimicrobial activity of zero-valent iron nanoparticles. Int J Mod Eng Res **2**(1), 578–581 (2012)
38. Tran, N., Mir, A., Mallik, D., Sinha, A., Nayar, S., Webster, T.J.: Bactericidal effect of iron oxide nanoparticles on *Staphylococcus aureus*. Int J Nanomed **5**(1), 277–283 (2010)
39. Touati, D.: Iron and oxidative stress in bacteria. Arch Biochem Biophys **373**(6), 1–6 (2000). doi:10.1006/abbi.1999.1518
40. Lee, C., Kim, J.Y., Lee, W.I., Nelson, K.L., Yoon, J., Sedlak, D.L.: Bactericidal effect of zero-valent iron nanoparticles on *Escherichia coli*. Environ Sci Technol **42**(13), 4927–4933 (2008). doi:10.1021/es800408u
41. Makhluf, S., Dror, R., Nitzan, Y., Abramovich, Y., Jelinek, R., Gedanken, A.: Microwave-assisted synthesis of nanocrystalline MgO and Its use as a bacteriocide. Adv Funct Mater **15**(10), 1708–1715 (2005). doi:10.1002/adfm.200500029
42. Zhang, L., Jiang, Y., Ding, Y., Povey, M., York, D.: Investigation into the antibacterial behaviour of suspensions of ZnO nanoparticles (ZnO nanofluids). J Nanopart Res **9**(3), 479–489 (2007). doi:10.1007/s11051-006-9150-1
43. Taylor, E.N., Webster, T.J.: The use of superparamagnetic nanoparticles for prosthetic biofilm. Int J Nanomed **4**(1), 145–152 (2009)